EFFECTS OF URBANIZATION AND CLIMATE CHANGE ON HYDROLOGICAL PROCESSES OVER THE SAN ANTONIO RIVER BASIN, TEXAS

A Thesis

by

GANG ZHAO

Submitted to the Office of Graduate and Professional Studies of
Texas A&M University
in partial fulfillment of the requirements for the degree of

MASTER OF SCIENCE

Chair of Committee,	Huilin Gao
Committee Members,	Francisco Olivera
	Steven M. Quiring
Head of Department,	Robin Autenrieth

December 2014

Major Subject: Civil Engineering

Copyright 2014 Gang Zhao

ABSTRACT

With the rapid population growth and economic development in the State of Texas, a fast urbanization process has occurred over the past several decades. The direct consequences of the increased impervious area are greater surface runoff and higher flood peaks. Meanwhile, climate change has led to more frequent extreme events. Therefore, a thorough understanding of the hydrological processes under urbanization and climate change is indispensable for sustainable water management. In this investigation, a case study was conducted by applying the Distributed Hydrology Soil Vegetation Model (DHSVM) to the San Antonio River Basin (SARB), Texas. Hosting the seventh largest city in the U.S. (i.e., City of San Antonio), the SARB is vulnerable to both floods and droughts. A set of historical and future land cover maps were assembled to represent the urbanization process. Two forcing datasets were employed to drive the DHSVM model. The first is a long-term observation based dataset (1915-2011), which was used as inputs for calibrating and validating DHSVM, as well as evaluating the urbanization effect. The second is the statistically downscaled climate simulations (1950-2099) from the Coupled Model Intercomparison Project Phase 5 (CMIP5), which were applied for understanding impacts related to climate change. Results show that urbanization exerts a much larger influence on streamflow than climate change does. Under the same observed forcings, annual average streamflow increased from 28.12 m^3/s (with 1929 land cover) to 50.34 m^3/s (with 2011 land cover). As for climate change, results suggest that it will exacerbate the drought severity — with reduced

evapotranspiration and soil moisture caused by decreased precipitation. However, the projected future streamflow does not show a clear increasing or decreasing trend. Regarding the combined effect from urbanization and climate change, the results indicate that the seasonal streamflow magnitude will be notably changed. Furthermore, with significantly decreased evapotranspiration and slightly increased soil moisture, more water will be available for streamflow, increasing the possibility of flood risk in the region.

ACKNOWLEDGEMENTS

First of all, I would like to thank my committee chair and advisor, Dr. Gao. She continuously gave me very helpful suggestions not only for my research but also for all other aspects in my life. I also want to thank my committee members, Dr. Olivera and Dr. Quiring for their valuable support throughout this research. My thanks also go to the assistant head of our department, Prof. Zhang as well as other faculty and staff who have been helpful. I am also very grateful for the help from my friends, including Shuai Zhang, Kyungtae Lee and my roommate Jian Jiao.

This work was supported by startup funds from the Texas A&M University College of Engineering and the Zachry Department of Civil Engineering. I acknowledge Dr. Ben Livneh for providing the historical forcings for this study. In addition, this study has also benefitted from the usage of the Texas A&M Supercomputing Facility (http://sc.tamu.edu). In general, my sincere gratitude goes to everything in Texas A&M University. I will never forget this precious experience as an Aggie.

Finally, I thank my mother and father for their endless encouragement which always give me inexhaustible power in my life.

TABLE OF CONTENTS

Page

LIST OF FIGURES

LIST OF TABLES

CHAPTER I

INTRODUCTION AND LITERATURE REVIEW

Surface hydrology plays an indispensable role in Earth's surface-biosphere-atmosphere system. However, despite its significance, our knowledge about this process is still limited because of its complexity and variability. Moreover, with human activity and the effects of global warming, a great deal of scientific evidence show that the natural hydrologic cycle has been remarkably modified, which could result in serious consequences such as catastrophic flood, severe droughts, etc. (Eastering et al., 2000). This situation ultimately poses an essential challenge to the sustainable protection of our water management system.

As urbanization spreads, the rainfall-runoff relationship is expected to be more variable due to the increasing percentage of impervious areas. Weng (2001) studied the runoff response to growing urban areas and reported an increased annual rainfall-runoff coefficient. Research conducted by Olivera and DeFee (2007) in the area northwest of Houston, Texas, demonstrated that urbanization contributed 77% of the 146% increase in runoff depth. The expansion of impervious surfaces causes less infiltration into the soil and more direct storm runoff, which subsequently increases flood risks (Sheng and Wilson, 2009). In addition, in urban areas, with a high coverage of impervious surfaces and a strong reduction of vegetation areas, losses due to evapotranspiration (ET) end to be smaller. In the suburbs of the Tokyo Metropolitan area, Kondoh and Nishiyama (2000) suggested ET will decrease about 62% when artificial land use increases from

22.1% to 37.1%. Typically, soil moisture will tend to be smaller if infiltration is reduced. On the other hand, impervious surfaces will diminish the soil water evaporation and reduced vegetation will cut down transpiration. Both of these factors can increase the soil moisture. Also, in most urban areas the proportion of impervious surfaces for different regions are varied based on the land use purposes (e.g., dense urban and light urban). However, these facts are poorly (or not at all) represented in most hydrologic models, which results in biased estimation of the effects from urbanization. Therefore, adoption of a physically based explicit hydrologic model is essential to provide quantitative evaluation of the effects from urbanization on hydrological processes.

Global climate change is another factor expected to play a key role in altering hydrological processes. Several studies have shown that significant changes of temperature and precipitation will occur as the result of climate change (Marengo et al., 2009; Beniston et al., 2007). Such changes will consequently cause many problems such as the rising of sea levels, the shifting of seasons, more extreme weather and climate events, etc. (Bates et al., 2008). These long term changes affect water resources to a great extent. Because of the complexity of the climate systems and the anthropogenic effects, it is practically impossible to completely predict future streamflows in an exact manner. In order to assist policy formation and implementation, many studies have been conducted over the past several decades. Among these studies, General Circulation Models (GCMs) have been widely applied and proved supportive to provide information about the changing climate (Stocker et al., 2013). Nevertheless, although the Intergovernmental Panel on Climate Change (IPCC) announced that GCMs are presently

the most advanced tools available for improving our understanding of climate change processes, GCMs cannot provide accurate and consistent information at a regional scale because of their relatively coarse spatial resolution and because of the different algorithms employed by each model. In addition, typical GCMs do not have a detailed representation of the hydrological processes (i.e., ET, soil moisture, runoff, etc.). Thus, a common practice is to drive hydrological models using spatially (and temporally) downscaled outputs from GCMs. The simulated results from the hydrological modeling are considered to be more reliable for use by policy makers in decision making.

Both urbanization and climate changes effects on the hydrologic cycle are being increasingly studied using hydrological modeling methods at regional scales. A study conducted by Jha et al. (2004) coupled a regional climate model and the Soil and Water Assessment Tool (SWAT) to evaluate the effect of climate change on streamflow in the Upper Mississippi River Basin (UMRB). The Long-Term Hydrologic Impact Assessment (LTHIA) model was used by Grove et al. (2001) in Little Eagle Creek, Indiana. Results showed average annual runoff depths have increased dramatically in the past several decades because of urbanization. Results from White and Greer (2006) in Los Penasquitos Creek, California suggested that the daily median and minimum, the dry season runoff, and the magnitude of flood flows have increased due to the growth of urbanized land. Another study by Cuo et al. (2011) investigated the change of flows over Puget Sound in the Pacific Northwest under urbaninzation and climate change, respectively. Despite the perspectives gained through the previous studies, knowledge about three important aspects is critically needed. First, understanding about the

combined effects of long-term urbanization processes and changing climate conditions is still limited. Second, few studies take both evapotranspiration (usually the largest loss of total precipitation) and soil moisture (an important indicator of drought) into consideration. Third, the urbanization effects across different scales within a given river basin are unclear.

The objective of this study is to evaluate the effect of urbanization and climate change on the hydrological processes (by testing all water budget terms) both separately and jointly. Specifically, answers for the following questions were explored:

1) If urbanization and climate change effects on hydrological processes compound, how do they weigh against each other?
2) For different soil and vegetation types, how will the water budget terms propagate over time due to urbanization and climate change?
3) At the subbasin and basin scales, how the streamflows respond to different climate and urbanization scenarios?

The dissertation is organized as follows. Chapter II introduces our study area. The model and data used are also summarized in this Chapter (II), while Chapter III explains the methodology. Specifically, simulation designs, which explain how the model was set up to achieve the objectives, are also contained in Chapter III. Chapter IV is our results section, which also includes the discussions. Finally, conclusions are summarized in Chapter V.

CHAPTER II

STUDY AREA, MODEL AND DATA

2.1 Study area

As a result of the fast economic development, the State of Texas hosts three of the top ten largest cities in the United States (i.e., Houston, Dallas, and San Antonio). According to population census data (U.S. Census Bureau, 2010), Texas has the largest urban area (22651 km^2) and the second largest urban population (21,298,039) in the country. In addition, the urban population of Texas keeps growing quickly with an increasing rate of 2.16% per year (from 2000 to 2010). It is projected that the urban population for major metropolitan areas in Texas will be nearly doubled by 2040 (Texas State Data Center, 2012). Compounded by climate change, this urban sprawl process will continuously contribute to the vulnerability of our environment.

The San Antonio River Basin (SARB, Figure 1a), located in southeast Texas (28.50-29.96°N, 96.89-99.61°W), is selected as our study area. It has a drainage area of 10,826 km^2 with an elevation ranging from 4 m to 693 m above sea level. The average annual rainfall is 768 mm. The dominant vegetation type in the SARB is grass while soil types are mainly clay and clay loam (Figure A-1 in Appendix A). There are six subbasins in the SARB including the Medina River Subbasin, the Leon Creek Subbasin, the Salado Creek Subbasin, the Upper San Antonio River Subbasin, the Cibolo Creek Subbasin, and the Lower San Antonio River Subbasin. The City of San Antonio, which is the seventh largest city in the United States, lies approximately in the middle of the

SARB. In the SARB, currently about 76% of the population resides in the City of San Antonio and its suburbs. With the rapid population growth and economic development in this area, a fast urbanization has been witnessed over the past several decades. However, the urbanization intensity of each subbasin varies considerably. Before the 1970s, the urban area of San Antonio City was mainly located in the Upper San Antonio River subbasin. Then it expanded to the Leon Creek and the Salado Creek subbasins. According to the 1970 land cover map, the urban area fraction in the Leon Creek, Salado Creek, and Upper San Antonio River subbasins was 7.0%, 13.2%, and 9.8%, respectively. By 2011, these fractions had increased to 25.7%, 35.2%, and 16.8%. In total, the impervious areas in the SARB expanded from 317.0 km^2 to 901.0 km^2 (1970 to 2011). The urban area expansion is closely related to the population growth. Figure 1b shows the relationship between the population and the urban area in the city of San Antonio during historical periods, which is used to estimate future urban area based on the projected population growth.

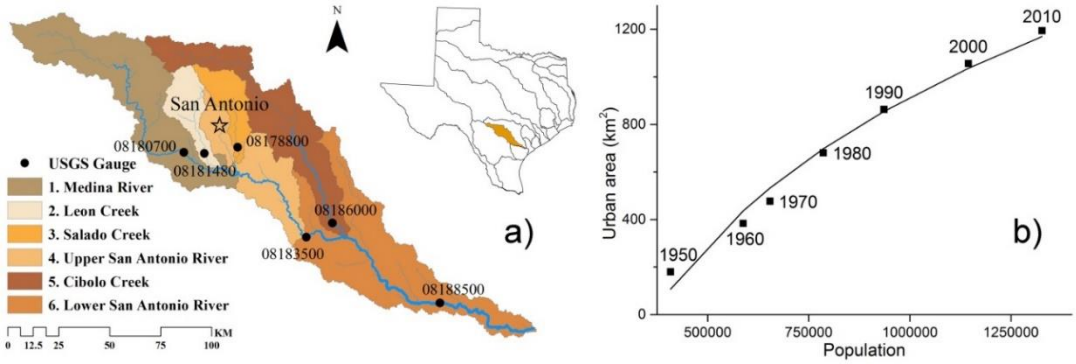

Figure 1. a) San Antonio River Basin and its six subbasins, b) the urban area-population relationship.

The streamflows of the San Antonio River are highly variable. According to U.S. Geological Survey (USGS) observed streamflow data at the basin outlet (gauge ID: 08188500), the mean and standard deviation of the discharges from 1939 to 2013 are 22.72 m^3/s and 60.02 m^3/s, respectively. Since the SARB is vulnerable to both droughts and floods, the interannual variations are significant. For instance, the annual mean discharge was only 7.92 m^3/s during the drought year of 2011, while it was 80.64 m^3/s during the wet year of 2002.

2.2 Model and data

The Distributed Hydrology Soil Vegetation Model (DHSVM) is a fully distributed hydrologic model developed at the University of Washington (Wigmosta et al., 1994). It explicitly simulates the water and energy balance based on topography and vegetation cover at a high spatial resolution (e.g., 10m to 200m). The model is physically based and dynamically represents the hydrological processes such as ET, snow processes, urban area detention, soil water dynamics, etc. The model can simulate streamflows at a subdaily time step for a multiyear period. DHSVM had been used successfully to study the effects of land cover and climate change on the hydrology of the Puget Sound basin in Washington State (Cuo et al., 2008, 2009, 2011; Vano et al., 2010).

The DHSVM input data includes a digital elevation map (DEM), a basin boundary mask, soil texture information, and land cover types. In this study, the DEM data was obtained from the Shuttle Radar Topography Mission (SRTM) with about 30

meters resolution (Jarvis et al., 2008), which was then resampled to 200m (i.e., model resolution for the SARB). Based on the DEM information and hydrometric station locations, the soil depth map, the river network, and the basin boundary mask were generated using Geographical Information System (GIS) tools. The soil texture information was acquired from the State Soil Geographic (STATSGO) Database (Miller and White, 1998) and resampled from 1km to 200m.

The National Land Cover Database (NLCD) (Vogelmann et al., 2001; Homer et al., 2007; Fry et al., 2011; Jin et al., 2013) created by the Multi-Resolution Land Characteristics Consortium (MRLC) in years 1992, 2001, 2006, and 2011 were obtained and processed for this study. Classified using Landsat satellite observations, these 30 m NLCD products contain consistent land cover types across the United States. In addition, based on historical land surface information during the 1970s and 1980s, the USGS published Enhanced Historical Land-Use and Land-Cover Data Sets (LC1970 for short) (Price et al., 2006). However, before 1970 and after 2011, there are no existing land cover maps that can be employed to represent the corresponding urban area. Therefore, we created three additional historical land cover maps (i.e., LC1929, LC1958, and LC1964), and two future land cover maps (i.e., LC2030 and LC2080), based on the existing information (with the procedure explained in Appendix B). To focus on the impacts from increased impervious areas due to urbanization, the non-urban land cover types were held constant (i.e., same as LC1970). Figure 2 shows the ten historical and future land cover maps.

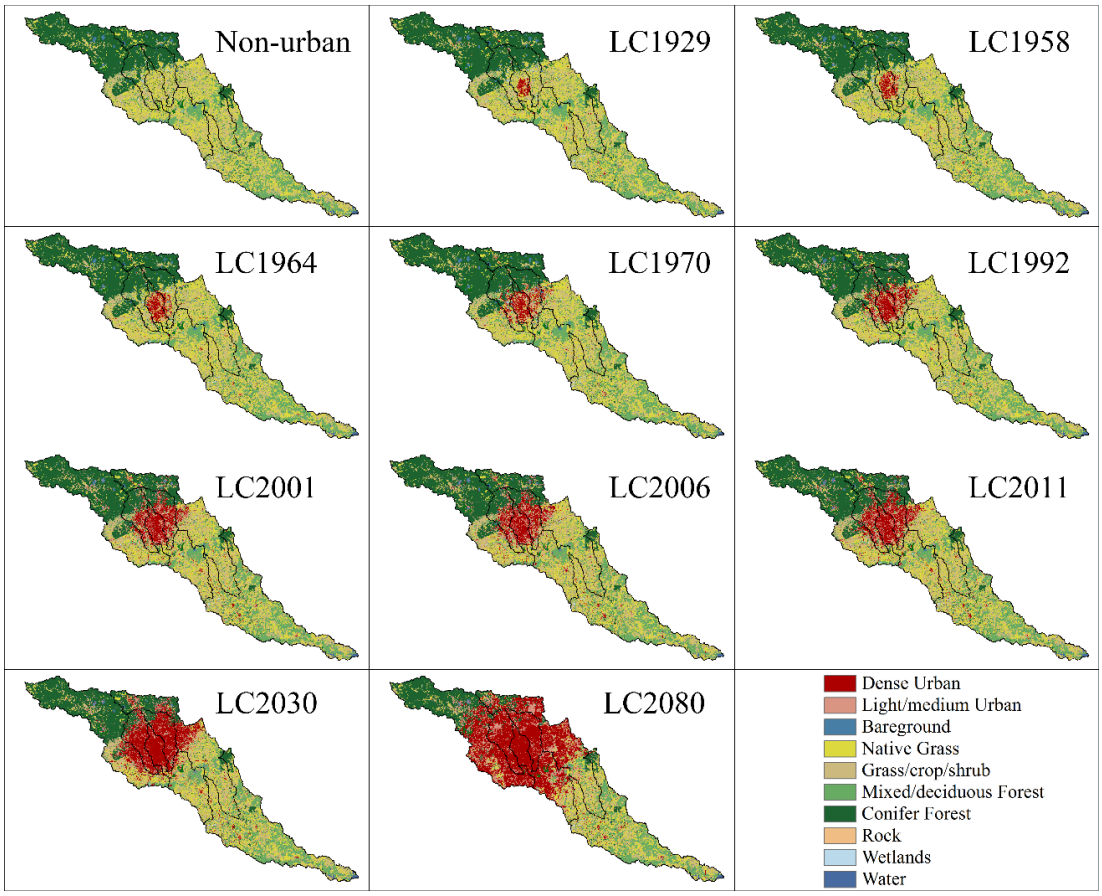

Figure 2. San Antonio River Basin land cover maps from 1929 to 2080.

Two forcing datasets were employed to drive the DHSVM model. For calibration and validation purposes, we utilized a long term observation based dataset by Livneh et al. (2013). This 3-hourly dataset from 1915 to 2011 covers the Continental United States at 1/16th degree spatial resolution. DHSVM forcings, including air temperature, wind speed, relative humidity, incoming shortwave radiation, incoming longwave radiation, and precipitation, were acquired from this dataset for the period of 1915 to 2011 for the SARB. These 1/16th degree forcings were further downscaled to the DHSVM model resolution (i.e., 200 m for this study) using the model's internal interpolation schemes.

In order to evaluate the effect of climate change, historical and future forcing data from the Downscaled Coupled Model Intercomparison Project Phase 5 (CMIP5) Climate and Hydrology Projections (DCHP) archive were acquired (Reclamation, 2013). This database contains monthly/daily precipitation and temperature data from 1950 to 2099. The spatial resolution of the DCHP dataset varies from 1/8th degree, to 1 degree, to 2 degrees. There are two statistical downscaling methods adopted by this dataset: monthly Bias Corrected Spatial Disaggregation (BCSD, Wood et al., 2002; Wood et al., 2004; Maurer et al., 2007) and daily Bias Correction Constructed Analogues (BCCA, Hidalgo et al., 2008; Maurer and Hidalgo, 2008; Maurer et al., 2010). For BCSD CMIP5 data with 1/8th degree spatial resolution, there are 39 models. For BCCA CMIP5 data with 1/8th degree spatial resolution, there are 21 models. Each of the 39 models with monthly data covers four Representative Concentration Pathway (RCP) scenarios (i.e., RCP 2.6, RCP 4.5, RCP 6.0, and RCP 8.5). For the 21 models with daily data, only 11 of them cover all of the four scenarios.

Since each CMIP5 model has its own physics and numerical methods, the outputs of different models vary enormously. A typical practice is to use the ensemble to represent the differences and similarities among these General Circulation Models (GCMs) and to analyze the uncertainty associated with these GCMs. However, for a hydrologic model with high spatial and temporal resolution (such as DHSVM), it is extremely computationally expensive to conduct simulations for each CMIP5 model. Therefore, it is important to choose a representative model that can appropriately characterize the past and future climate from the CMIP5 model ensemble. Given this

consideration, the following steps were taken for identifying a representative model. First, monthly precipitation and temperature over the SARB from all 39 CMIP5 models were utilized to calculate the ensemble means (of precipitation and temperature) over three 30-year periods (1970-1999, 2020-2049, 2070-2099) for each RCP scenario (Figure 3a, 3b) and each month (Figure 3c, 3d). Then, the results from each of the 11 models (which have daily data available) were compared with the ensemble means. The model which was most similar to the ensemble means (in terms of values and overall trends) was selected to drive the DHSVM simulations. In this case, the Norwegian Earth System Model (NorESM1-M, Bentsen et al., 2013; Iversen et al., 2013) was chosen to represent the averaged climate from CMIP5 models over the SARB.

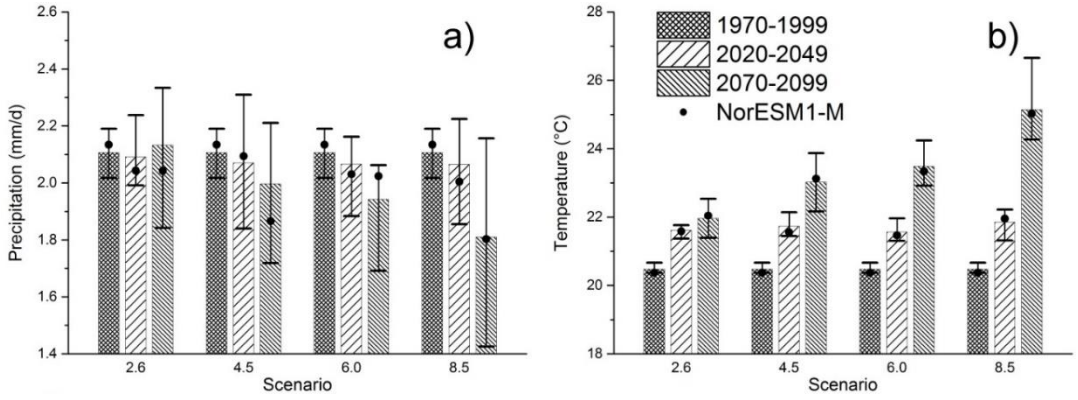

Figure 3. Precipitation and temperature from the CMIP5 models during three 30-year periods: (a) annual total precipitation; (b) mean annual air temperature; (c) monthly precipitation; and (d) monthly air temperature. The ensemble means are represented by the shaded bars. The maximum/minimum values from the ensemble are represented by whiskers, and the NorESM1-M results are denoted by dots.

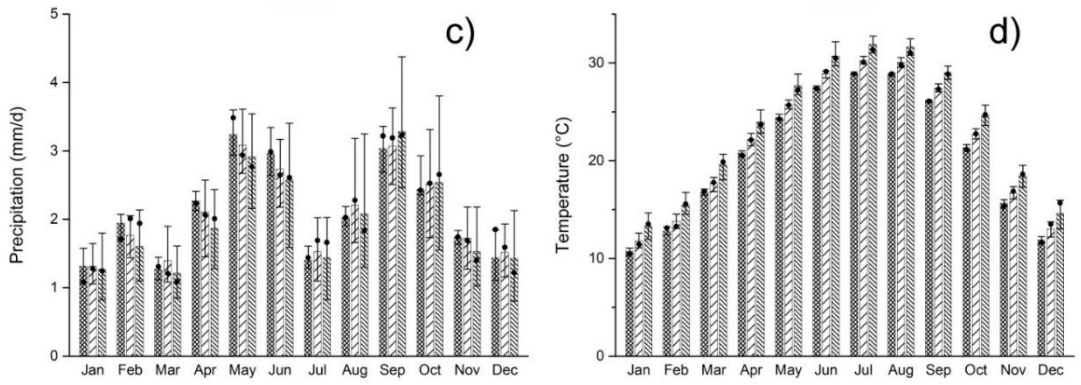

Figure 3. Continued.

Daily NorESM1-M model outputs from the DCHP database include precipitation, maximum temperature, and minimum temperature. Other forcing variables required by DHSVM such as shortwave radiation, longwave radiation, and air temperature were generated using the same method as described in Livneh et al. (2013). For wind speed, we assumed there is no significant change in the future. Thus, future wind speed values were adopted from historical data.

CHAPTER III

METHODOLOGY

3.1 Model calibration and validation

The DHSVM model was calibrated during the period from January 1, 1996 to December 31, 2000. Considering the different land cover and soil types among the six subbasins, each subbasin was calibrated separately. To avoid errors associated with upper basin calibrations affecting the lower basin calibrations, an inlet flow module was added to the latest version of DHSVM (i.e., version 3.1.1) which used the observed outflow from the closest upper basin as an independent forcing. In this module, DHSVM read the observed streamflow from upstream at each time step (along with the meteorological forcing variables) to simulate the flows in the studied downstream subbasin. Using this module, we were able to maximize the calibration accuracies at all subbasins and enhance the model performance across the entire SARB. Soil parameters (porosity, wilting point, vertical conductivity, and maximum infiltration) and vegetation parameters (detention fraction, detention decay, monthly leaf area index (LAI), canopy resistance, and vapor pressure deficit) were calibrated based on comparisons between simulated daily streamflows and USGS observations. Figure 4 compares the calibrated streamflows with observations at each of the subbasins. The statistical variables used for evaluating the results include relative bias, coefficient of determination (R^2), and Nash–Sutcliffe efficiency (NSE, Nash and Sutcliffe, 1970).

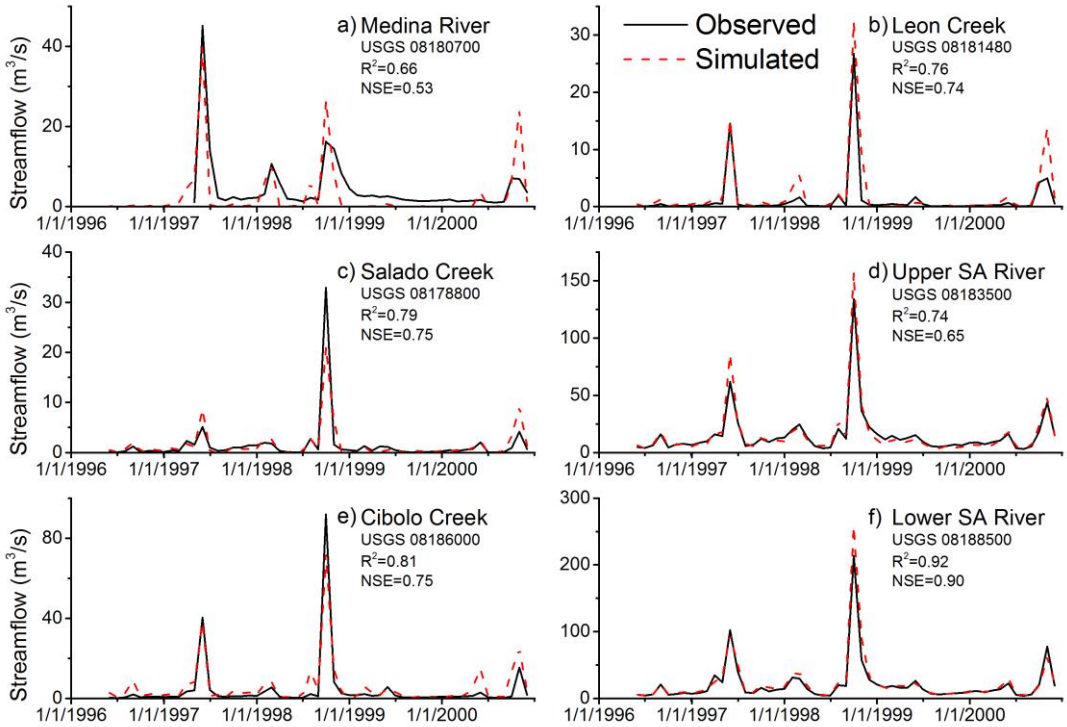

Figure 4. Calibration results for each subbasin.

Table 1. Validation results of the entire SARB (1996-2001)

Period	USGS gauge	Observed mean (m^3/s)	Simulated mean (m^3/s)	R^2	NSE
1950-1959	08188500	447.4	401.9	0.67	0.52
1960-1969	08188500	626.5	604.3	0.67	0.46
1970-1989	08188500	914.9	573.8	0.66	0.39
1990-1995	08188500	1176.8	1046.3	0.81	0.78
1996-2000	08188500	748.3	890.6	0.86	0.78
2001-2005	08188500	1627.6	1546.2	0.81	0.76
2006-2010	08188500	940.4	1106.6	0.59	0.36

The validation period was selected from January 1, 1950 to December 31, 2010. First, subbasins which do not have inlet flows from upper subbasins (i.e., Medina River,

Leon Creek, and Salado Creek) were simulated. Then, the Upper San Antonio River subbasin and the Cibolo Creek subbasin were modeled by accounting for the streamflow outputs from the three upper subbasins. Finally, the Lower San Antonio River subbasin was simulated to estimate the streamflows at the basin outlet. For each different validation period, the corresponding land cover map was used. All other parameters, regardless of whether calibrated or prescribed, were kept constant over time. Particularly, from January 1, 1996 to December 31, 2000 (i.e., the calibration time period), the model was re-run using inflow data from upstream subbasin outputs to validate the parameters for the entire SARB. Table 1 shows the validation results. The averaged R^2 and NSE from 1950 to 2010 are 0.71 and 0.63, respectively. The validation results suggest that the DHSVM model performs well over the SARB.

3.2 Model simulation designs

After calibration and validation, a suite of DHSVM model simulations were conducted for evaluating the urbanization and climate change effects on SARB surface hydrology.

To identify the urbanization effect, DHSVM simulations were conducted by changing land cover maps while using the same meteorological forcings. Specifically, we applied the same forcing data (Livneh et al., 2013) from 2001 to 2006 to ten different land cover maps from 1929 to 2080.

In order to isolate the effects of climate change, the land cover map was fixed to LC2001 while four sets of NorESM1-M forcings under different RCP scenarios were

employed (as forcing data). DHSVM simulations were conducted from 1950 to 2099. To capture the changing trends over the 150 years, we chose three 30-year periods (1970 to 1999, 2020 to 2049, and 2070 to 2099) to analyze the model results. The first period (i.e., 1970 to 1999) was selected as the baseline run, and the other two periods were chosen to evaluate future variations.

The combined effects, which represent the past and future more realistically, were analyzed by incorporating urbanization and climate change scenarios simultaneously. For each of the three 30-year periods (as defined earlier), land cover maps from 1970, 2030, and 2080 were used. Although within each of these 30-year periods the urban areas change with time, we chose these three particular land cover maps to simulate the long term changes (1970 to 2099). The DHSVM input data used for model calibration, validation, and impact analysis are summarized in Table 2.

Table 2. Summary of the DHSVM inputs used for model calibration, validation, and urban/climate change impact analysis.

Process	Land cover map	Forcing source	Scenarios	Period
Calibration	LC1992	Livneh et al., 2013	/	1996-2000
Validation	LC1958	Livneh et al., 2013	/	1950-1959
	LC1964			1960-1969
	LC1970			1970-1989
	LC1992			1990-1999
	LC2001			2001-2006
	LC2006			2006-2010
Urbanization	Non-urban	Livneh et al., 2013	/	2001-2006
	LC1929			
	LC1958			
	LC1964			
	LC1970			
	LC1992			
	LC2001			
	LC2006			
	LC2011			
Climate change	LC2001	NorESM1-M	RCP 2.6 RCP 4.5 RCP 6.0 RCP 8.5	1970-1999
				2020-2049
				2070-2099
Combined effect	LC1970	NorESM1-M	RCP 2.6 RCP 4.5 RCP 6.0 RCP 8.5	1970-1999
	LC2030			2020-2049
	LC2080			2070-2099

CHAPTER IV

RESULTS AND DISCUSSIONS

4.1 Urbanization effects

Land cover type changing from vegetation to impervious areas will significantly influence the runoff process and the magnitude of streamflows. Table 3 shows simulated streamflows under different historical and future urban scenarios. Both the mean and standard deviation of the streamflow increase along with increasing impervious area. From 1929 to 1964, mean streamflow increased slightly from 28.12 m^3/s to 29.67 m^3/s (0.044 $m^3 \cdot s^{-1}$/year), and standard deviation increased from 108.82 to 109.96 m^3/s (0.033 $m^3 \cdot s^{-1}$/year). However, from 1964 to 2011, mean streamflow and standard deviation increased to 50.34 and 141.45 m^3/s (0.44 and 0.67 $m^3 \cdot s^{-1}$/year), respectively. If the urban area keeps expanding as the population grows in the future, mean streamflow will increase at a rate of 0.60 $m^3 \cdot s^{-1}$/year from 2011 to 2080. An analysis of variance (ANOVA) was conducted to compare the mean values of urban streamflow with non-urban streamflow. P-values were shown in Table 3. From LC1970 to LC2080, the p-values are smaller than 0.011 (<0.05). This denotes that the growth in urban area since 1970 (with an impervious percentage of 2.93%) has a significant effect on the streamflows at the outlet of the SARB. Similar to the trends observed with mean and standard deviation, the magnitude of annual peak flows (Table 3) also increase - which means that the risk of flood events will be remarkably higher as the urbanization process continues. This is mainly because more infiltration excess runoff is generated due to

greater impervious surfaces. Therefore, during rainfall events, streamflow becomes flashier and peak discharge rates are magnified.

Table 3. Urbanization effects over the SARB on mean streamflow (p value in the parenthesis), standard deviation (STD) of streamflows, and average annual peak flows.

Land Cover Map	Impervious area (km^2)	Mean Flow(m^3/s)	STD (m^3/s)	Peak Flow (m^3/s)
non-urban	0.00	25.7 (-)	107.1	699.3
LC1929	72.44	28.1 (0.282)	108.8	712.0
LC1958	155.40	29.1 (0.138)	109.5	716.9
LC1964	225.56	29.7 (0.082)	110.0	720.9
LC1970	316.96	31.7 (0.011)	113.4	750.1
LC1992	448.08	36.7 (0.001)	120.7	805.0
LC2001	765.00	47.9 (0.000)	138.2	922.2
LC2006	815.05	48.9 (0.000)	139.8	932.8
LC2011	900.98	50.3 (0.000)	141.5	942.3
LC2030	1484.40	61.2 (0.000)	156.4	1034.4
LC2080	2906.39	92.0 (0.000)	202.8	1261.4

To evaluate the urbanization effect on streamflows over different regions and scales within the SARB, results under four urban scenarios over five representative locations were compared (Figure 5). The watershed above Location 1 is in the upstream region of urban areas. The watershed above Location 2 was urbanized as early as 1929, while watershed associated with Location 3 started to become urban around 1970 and (according to projections) will be completely urbanized in about 2080. The effect of urbanization on downstream channels can best be represented by the results for Locations 4 and 5. For Location 1, there is little change with the streamflow due to little land cover change. For Location 2, since the urban areas expanded from 1929 to 2001

(with light/medium urban areas converted to dense urban areas), a clear increase in the quantity of steamflows from 1929 to 2001 is observed. After 2001, the streamflows basically remains the same because urban area has peaked (in 2001).

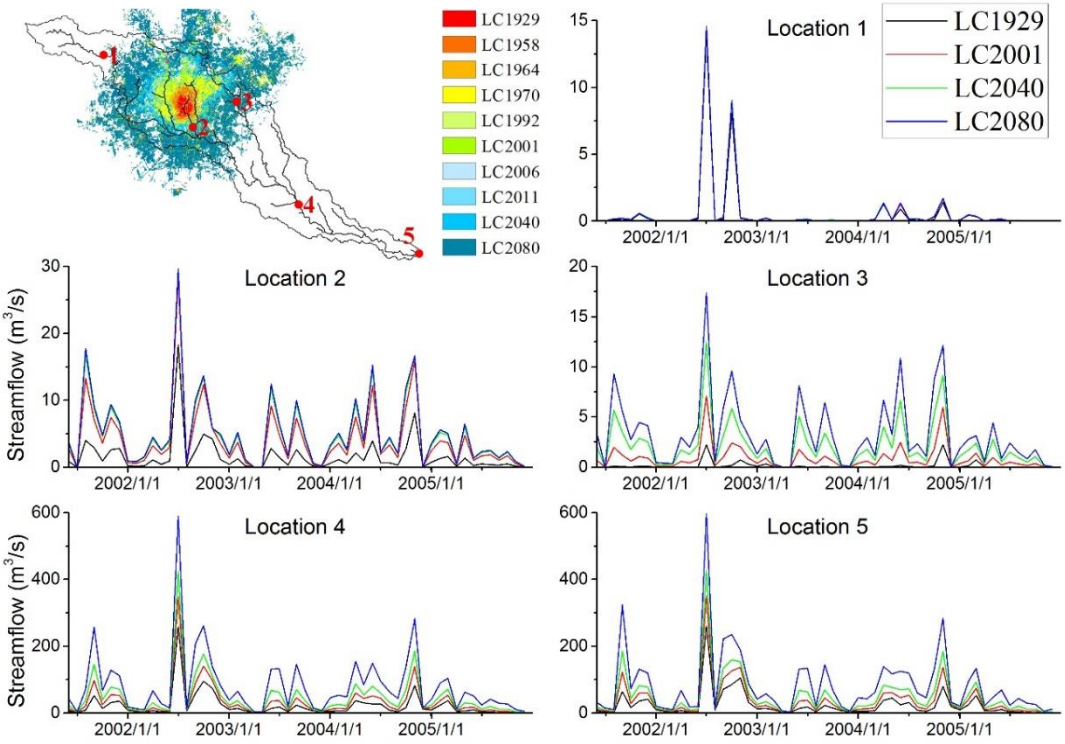

Figure 5. Comparison of streamflows at different locations from simulations of 4 land cover maps.

Results at Location 3 represent the effect of land cover changes from non-urban to dense urban area. With continuous urbanization, the streamflows keep increasing over time. The average incremental percentages of increase in mean streamflows are 2.45%/year, 3.07%/year, and 0.92%/year for the periods 1929 to 2011, 2011 to 2030, and 2030 to 2080, respectively. With the slowing down of the urbanization process after

2030 in the watershed above Location 3, the increasing percentages are expected to be reduced. The time series results of Location 4 have similar incremental percentage values as Location 3. At the outlet of the SARB (Location 5), it shows the same pattern as with Location 4. Comparing the peak flows of Locations 4 and 5, it suggests that the contributions of the downstream subbasins to peak flows are very limited. This reveals that the effects of upstream urbanization on streamflow transfer all the way downstream until reaching the outlet. Using the LC2080 result as an example, the proportions of the peak flow event in July 2002 resulting from upstream urban area expansions for Locations 4 and 5 are 56.4% and 56.1%, respectively.

4.2 Climate change effects

Driven by the NorESM1-M forcings, DHSVM simulations were employed to study the climate change effects on the water budget terms such as streamflows, ET, and soil moisture. Figure 6 shows the statistics related to streamflows under different RCP scenarios by period. The results suggest that there is no apparent trend between different periods in terms of mean streamflow. Although temperature will keep increasing, there are still large uncertainties in the projected future precipitation, which is the key driver of streamflows. With respect to the standard deviation, there will be a small decrease from 2020-2049 and then an increase from 2070-2099. Using RCP 4.5 as an example, standard deviation will first decrease from 50.68 m^3/s to 46.30 m^3/s and then increases to 64.05 m^3/s. With regards to average annual peak flow, it generally shares the same trend as with the mean flow. In order to analyze the low flow trend, the 5^{th} percentile of the

historical USGS observed streamflow data at the SARB outlet (USGS gauge 08188500, from March 1, 1939 to March 1, 2013) was used as the threshold for defining low flows. Subsequently, the total number of low flow days for each simulation period was divided by the number of low flow events to get the mean consecutive low flow days. According to Figure 6d, low flow days increase in Period 2 and Period 3 (as compared with Period 1), which indicates that drought conditions will be worse in the future.

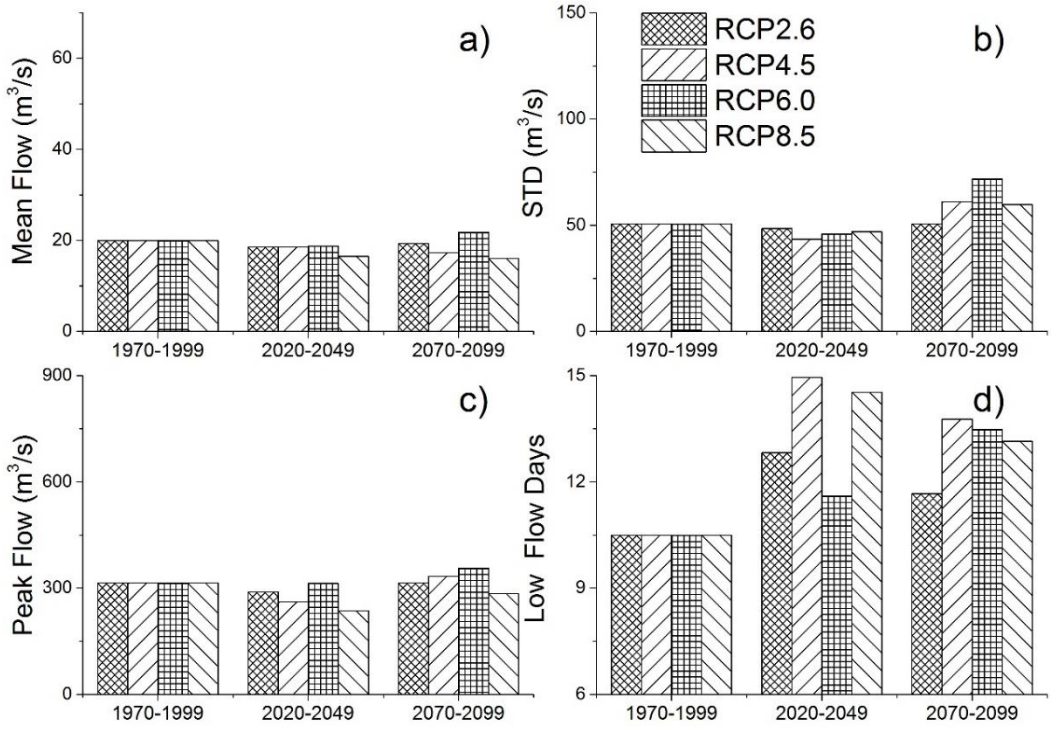

Figure 6. Climate change effects on streamflows over the SARB: (a) Mean; (b) Standard deviation; (c) Peak flow; and (d) Low flow days.

Results from the RCP 4.5 scenario were used as an example to evaluate the climate change impacts on monthly streamflow, annual ET, and soil moisture. Because

NorESM1-M projected monthly precipitation - which is very close to the CMIP5 ensemble mean – barely changes (Figure 3c), little change can be noticed with the resulted monthly streamflow (Figure 7). Similarly, the decreased streamflows in May are primarily due to the decrease in precipitation during this month (Figure 3c).

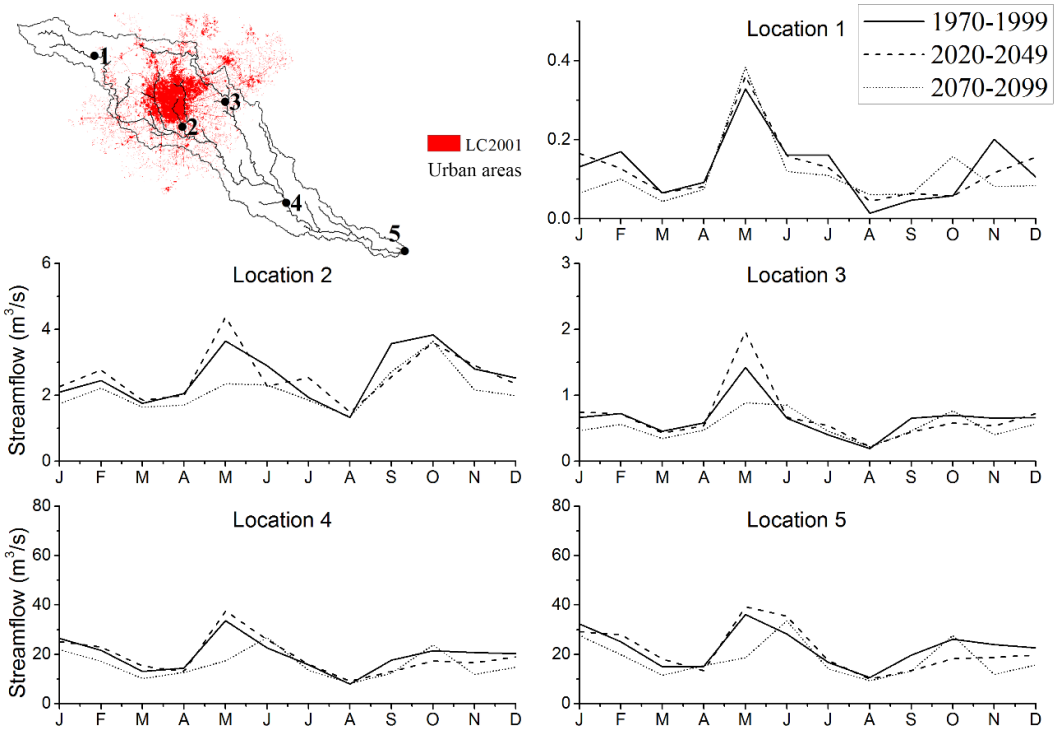

Figure 7. Monthly mean streamflows at different locations for the RCP 4.5 scenario (with 2001 land cover).

Figure 8 geographically shows the 30-year mean ET and soil moisture during these three periods. For ET, there is a clear distinction between different soil textures and vegetation types. Particularly, for sand soil, ET is relatively low over all three periods because water in sand soil drains quickly down to a deeper layer or to adjacent

lower elevation grid cells. A similar pattern is also observed over the urban areas, where the impervious surface is both 1) covered by little vegetation, and 2) prevents water evaporation from the underlay soil. With respect to the entire SARB, average ET decreases 4.3% from Period 1 to Period 2, and 12.6% from Period 2 to Period 3 because of the decrease in precipitation during the RCP 4.5 scenario. Although increasing temperature will enhance the potential ET, smaller precipitation will overweigh the warming effect. With regard to soil moisture, soil texture is the major influencing factor. Sand soil results in both the lowest ET and the smallest soil moisture. In contrast, silty clay has relatively higher soil moisture. In the region where the soil is clay, the non-uniform soil moisture is mainly due to impervious coverage in the urban areas. Since the low infiltration rate in urban soil is compensated by greater ET reduction, soil moisture values are generally higher than the surrounding areas. This results are also consistent with Rahman et al. (2014) and the soil moisture observation data across the U.S. (Appendix C). Similar with ET, as the precipitation decreases in Period 3, the soil moisture will also decrease in urban areas. However, for other land cover types, soil moisture mostly remains unchanged even though precipitation is decreasing. This means that soil moisture is more sensitive in urban areas, which should be considered as a factor in future urbanization projections.

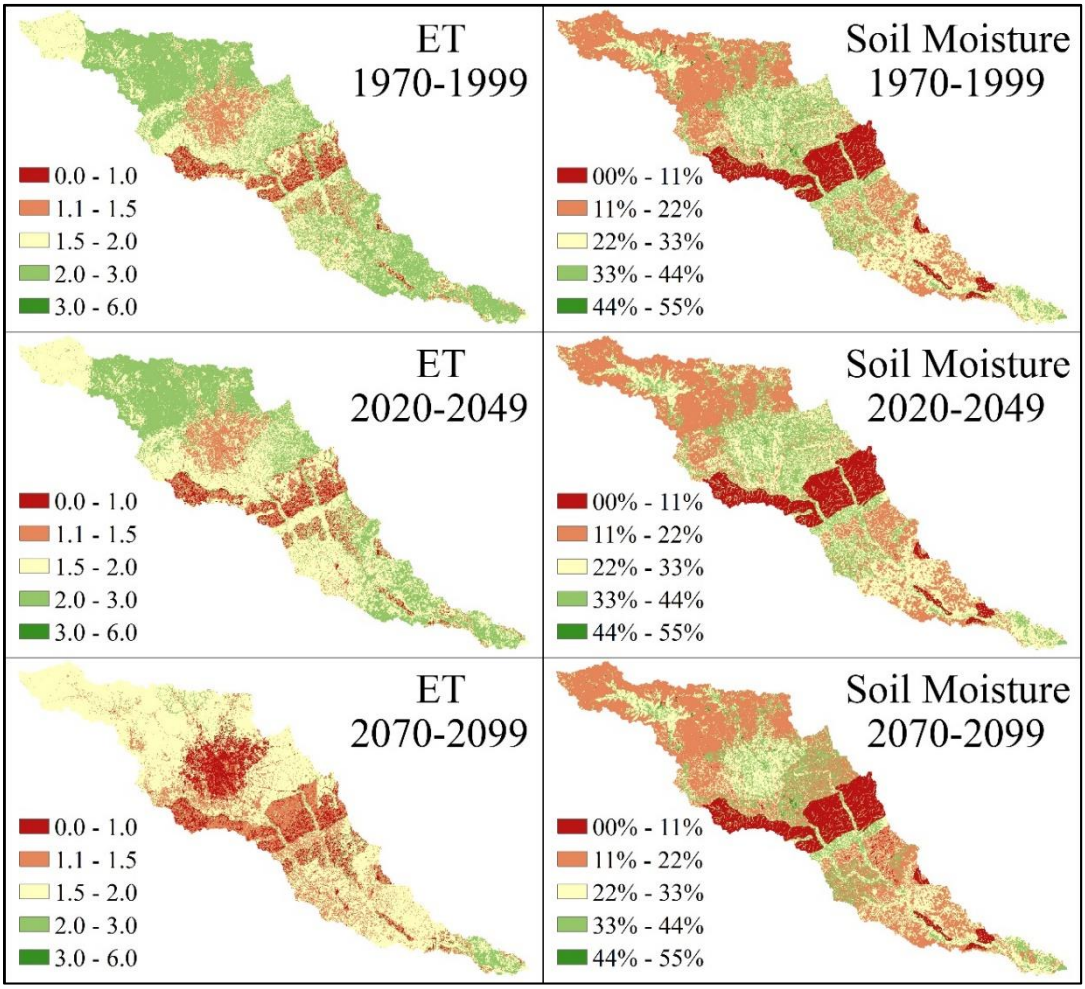

Figure 8. ET (mm/day) and volumetric soil moisture distribution over the SARB for 3 simulation periods (climate change).

4.3 Urbanization and climate change combined effects

Since urbanization and climate change occur simultaneously, evaluation of their combined effects is essential for practical water management decision making. To study these combined effects, the same forcing inputs from the NorESM1-M model were used while a representative land cover map was selected for each period: LC1970 for Period 1, LC2030 for Period 2, and LC2080 for Period 3.

Figure 9 shows the results of combined effect on streamflow. The trends of mean streamflow, standard deviations, and average annual peak flows share the same pattern over time (i.e., trend between different periods) with those under climate change alone (Figure 6). However, the average streamflow values of Period 1 decrease from 19.98 m^3/s to 13.99 m^3/s. This is because NLCD 2001, which was used in the climate change alone simulation, was replaced by a land cover map that is consistent with the simulation period. This also explains the significant increase with the streamflows in Period 2 and Period 3. Different from the effect of climate change alone, standard deviation will increase over time. This indicates that urbanization will make streamflows more variable, mainly because of the enhanced magnitude of high flows (shown in Figure 9c for peak flow). With respect to average consecutive low flow days, the combined effect has an opposite trend (i.e., decreasing) compared with the climate change alone effect. This result indicates that low flow will also be amplified by urbanization in the SARB– an effect that is consistent with the findings over Puget Sound River Basin by Cuo et al. (2008).

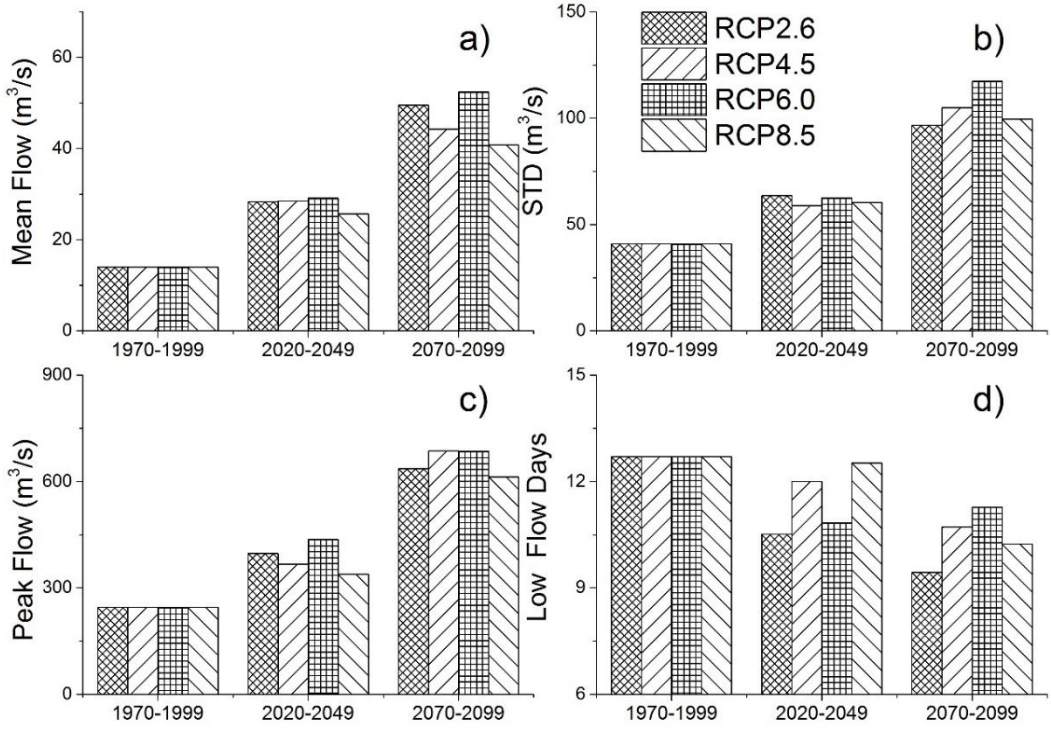

Figure 9. Combined effects (urbanization and climate change) on streamflows over the SARB: (a) Mean; (b) Standard deviation; (c) Peak flow; and (d) Low flow days.

Monthly changes of streamflows under the RCP 4.5 scenario over different locations are shown in Figure 10. There is no clear change with the streamflow at Location 1 because it is located above the urban areas. At other locations, due to the magnified effect caused by urbanization, streamflows are elevated dramatically during Period 2 and Period 3. However, each month has a different magnitude of change. This is mainly because of the seasonal—as well as long-term—variability associated with NorESM1-M forcing data.

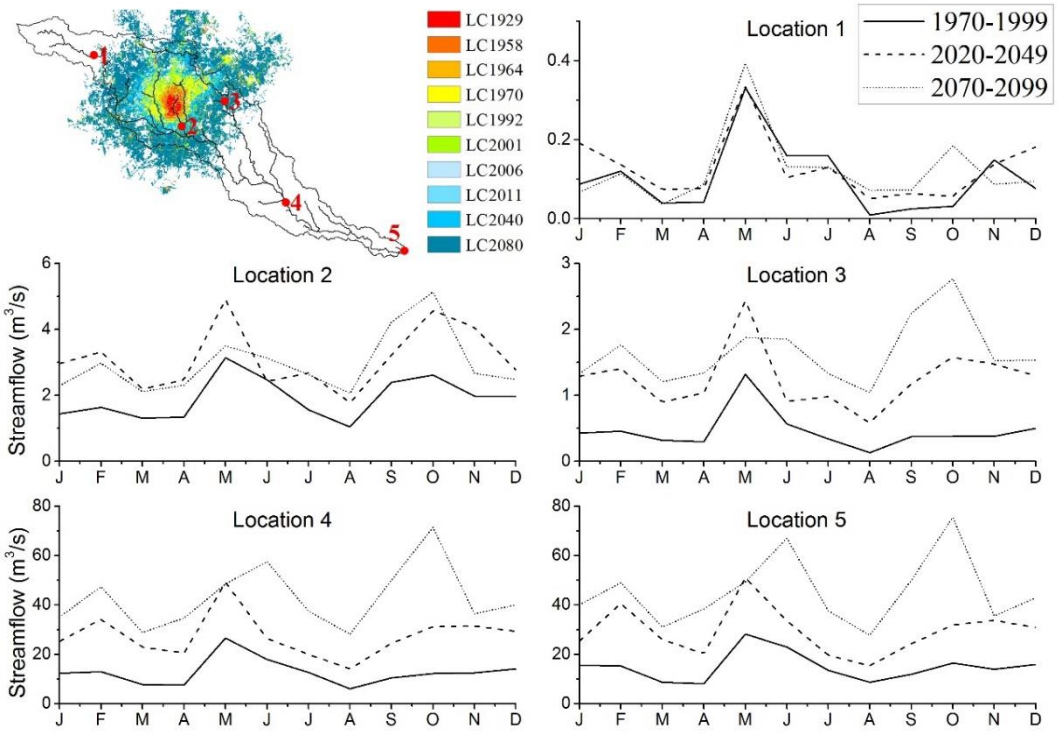

Figure 10. Monthly mean streamflows at different locations for the RCP 4.5 scenario (with different land cover maps for different periods).

Spatially distributed ET and soil moisture images for each period are shown in Figure 11. Compared with the results from climate change alone (Figure 8), a dominant urban expansion effect can be observed. Impervious surfaces remarkably decrease the ET and slightly increase soil moisture. For example, the average soil moisture increases 4.7% (relatively) while ET decreases 28.5% from Period 1 to Period 3. The increase of soil moisture mostly comes from urbanization. Similarly, these results are also consistent with Rahman et al. (2014) and with observations (Appendix C). As a consequence of largely decreased ET, more water from precipitation will be routed to the river channel, which will significantly increase the streamflow values. On the other hand, with ET

decreasing, latent heat will decrease, leading to higher temperatures in the city (i.e., urban heat island).

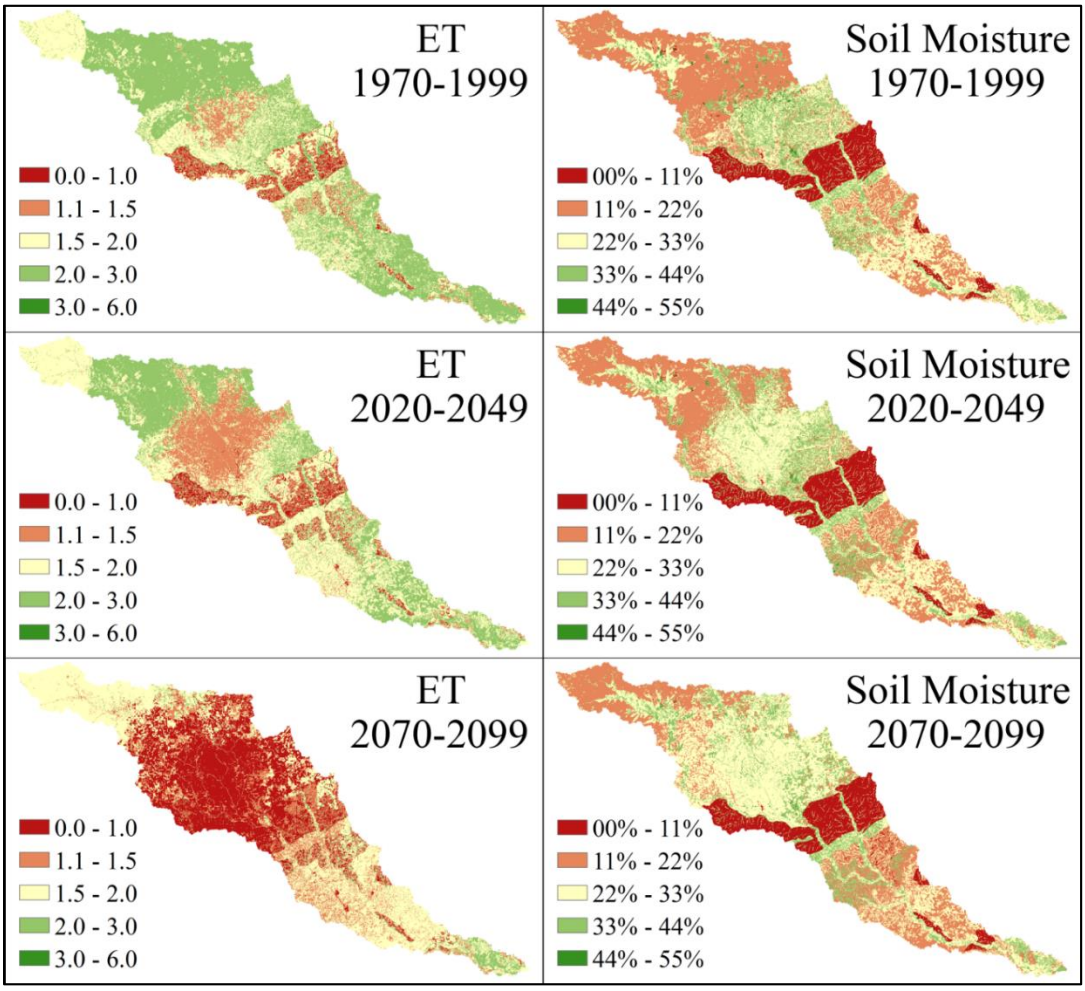

Figure 11. ET (mm/day) and volumetric soil moisture distribution over the SARB for 3 simulation periods (combined effect).

4.4 Discussions

Results show that both urbanization and climate change will alter the hydrological processes and the water budget. However, the impact from urbanization is

considerably larger than climate change in the SARB. Using RCP 4.5 as an example, without urbanization, the 30 year average streamflow will decrease 7.07% from Period 1 to Period 2 and 7.08% from Period 2 to Period 3. Our results suggest, however, that under urban expansion streamflows will increase 103.83% and 55.24%, respectively. The simulations of this study can also be implemented in other urbanized basins. Based on the results from this study, policy makers can better formulate policies focusing on the methods to diminish the effect from urbanization. For example, Low Impact Development (LID), which employs sustainable storm water principles to minimize the imperviousness effect, has been adopted in many regions (Dietz, 2007).

Like the other modeling studies, there are some uncertainties associated with the model input data, the model structure, and model parameters. Specifically, for the urbanization process population growth is the key driver. However, factors such as immigration policy, economic development, technology, etc. will make the rate of urbanization variable. Additionally, because our intention in this study was only to examine urbanization effects, hydrological impacts from other land cover type changes (e.g., agricultural expansion, deforestation) are not investigated.

Uncertainties associated with the forcings generated by GCMs depend on uncertainties in the chemical, physical, and social models involved, as well as modeling structures and numerical methods adopted (Hawkins and Sutton, 2011; Murphy et al., 2004; New and Hulme, 2000). Although the NorESM1-M model agrees well with the CMIP5 ensemble means, it is necessary to address the uncertainty due to the differences from these GCMs. In the future climate scenarios, the sources of uncertainties are mainly

precipitation and temperature. Therefore, in this study, we quantified the uncertainties in streamflow, ET, and soil moisture that come from precipitation and temperature. First, ensemble mean values of the 11 GCMs (with four scenario daily data) were calculated, in which the maximum and minimum values were selected to compare with NorESM1-M. Taking Period 2 from RCP 4.5 as an example, the NorESM1-M has an average precipitation value of 1.95 mm/day and the maximum and minimum precipitation are 2.20 mm/day (+12.7% comparing with 1.95, CCSM4.0) and 1.82 mm/day (-6.7%, GFDL-ESM2G). For average temperature, NorESM1-M has a value of 21.95°C and the maximum and minimum values are 22.51°C (+0.56°C, MIROC-ESM-CHEM) and 21.72°C (-0.23°C, MIROC-ESM). Then, based on the maximum and minimum values, we perturbed the NorESM1-M daily precipitation by -5%, +5%, and +10% and the temperature by -0.5°C and +0.5°C, respectively. Figure 12 shows the results for the SARB. For ET, soil moisture, and streamflow, the precipitation elasticity (Vano et al., 2012; first defined in Schaake, 1990) are 0.79, 0.39, and 2.73, respectively. With the increase of precipitation, ET, soil moisture, and streamflow will all increase–but different months will have various change magnitudes. For instance, streamflow in May will increase more than in August while ET increases more during the warm season (April to October) than in cold season (November to March). With respect to temperature sensitivity (Figure 12b), little change can be observed. This is because in the SARB, precipitation is the dominant factor. Though temperature increases slightly, if there is not enough rainfall water, ET and soil moisture will stay constant. As the consequence, streamflow will also remain the same. In summary, we analyzed the four

RCP scenarios which represent greenhouse gas emission uncertainties and the uncertainties associated with precipitation and temperature among different climate models.

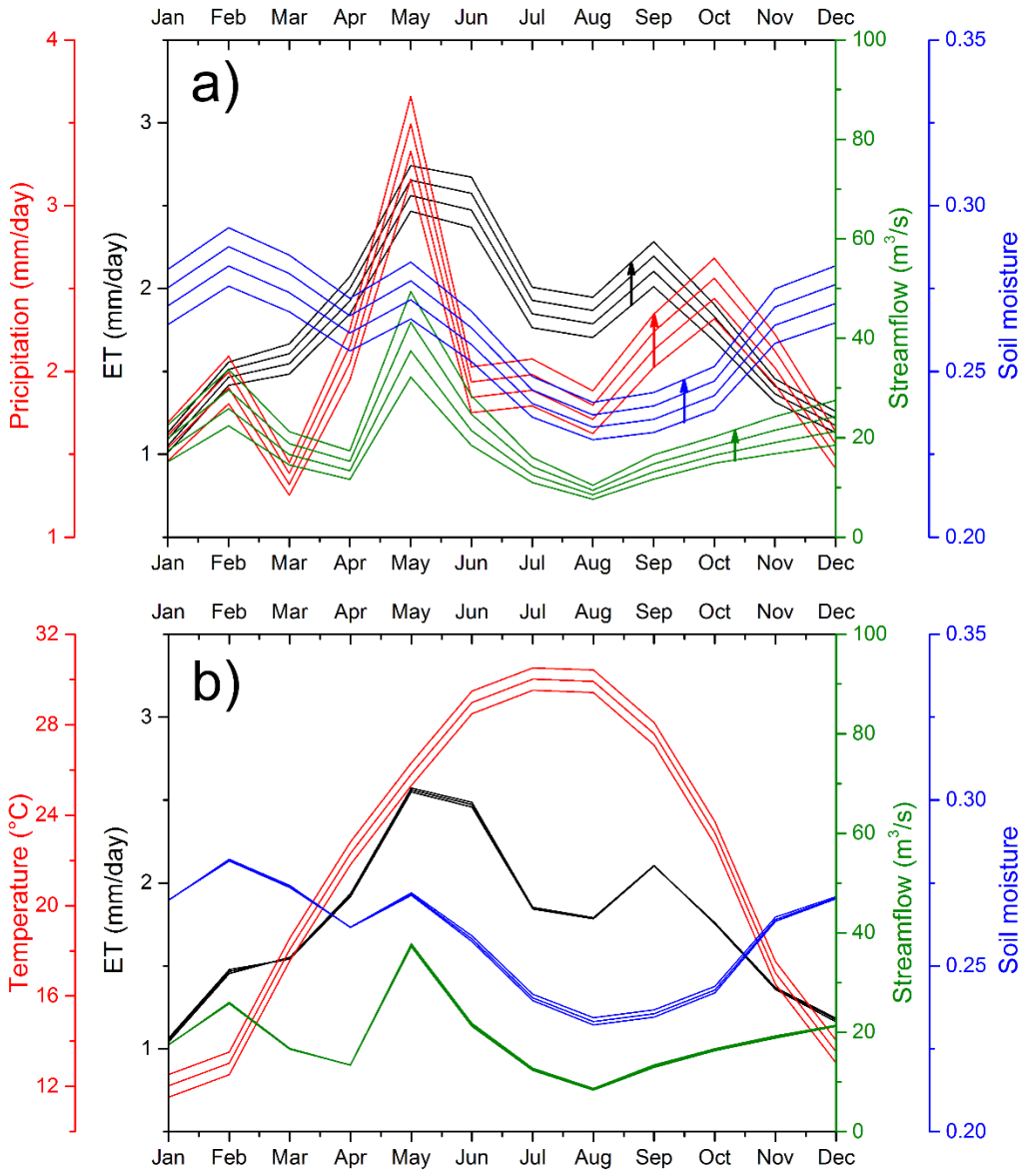

Figure 12. Uncertainties for precipitation and temperature for 2020-2049 from RCP 4.5.

CHAPTER V

CONCLUSIONS

The objectives of this study were to evaluate the effect of climate change and urbanization on hydrological processes under various scenarios. The San Antonio River Basin was selected as our research area because this basin is not only experiencing fast urban area expansion but is also undergoing changing climate. In order to represent progressive urbanization in the basin, three historical and two future land cover maps were generated for this study. Together with the existing land cover maps, 10 land cover maps were utilized to investigate the effect of urbanization. With respect to climate change, the statistically downscaled NorESM1-M model outputs from DCHP were selected to represent the CMIP5 models.

The results show that the effect of urbanization on hydrological processes is much larger than that of climate change. Streamflow (as well as the variability of streamflow) is remarkably elevated due to increased impervious surface area. This means higher flood risk in the river channel as the urbanization process continues. In addition, different locations in the river have various responses to the expansion of urban areas. For the climate change effect, there is no clear trend with the streamflow. However, if precipitation decreases, ET and soil moisture will both decline. Finally, NorESM1-M forcing data with changing land cover maps were used as inputs for DHSVM to investigate the combined effect due to urbanization and climate change. The results suggest that the streamflow will increase significantly under all four RCP

scenarios. Clear changes in both ET and soil moisture due to urban expansion can be observed. ET will decrease since construction of urban areas will block evaporation from soil and reduce transpiration from vegetation. Since the reduction of ET overweighs the reduction of infiltration, soil moisture will increase slightly.

To best represent the hydrological uncertainties associated with different GCMs, a series of simulations with perturbed forcings were conducted. Results suggest that uncertainties associated with precipitation are much larger than those associated with temperature. The precipitation elasticity for ET, soil moisture, and streamflow are 0.79, 0.39, and 2.73, respectively.

In general, because sustainable water resource management is a big issue facing human beings, influencing factors of water resources need to be urgently investigated. This study provides a quantitative evaluation of the hydrological responses to urbanization and climate change, which can provide helpful information to policy makers to regulate our valuable water resources more reasonably.

REFERENCES

Bates, B., Z. W. Kundzewicz, S. Wu, and J. Palutikof (2008), Climate change and water, Intergovernmental Panel on Climate Change (IPCC), IPCC Technical Paper VI, 210 pp.

Beniston, M., D. B. Stephenson, O. B. Christensen, C. A. Ferro, C. Frei, S. Goyette, K. Halsnaes, T. Holt, K. Jylhä, and B. Koffi (2007), Future extreme events in European climate: an exploration of regional climate model projections, Climatic Change, 81(1), 71-95.

Bentsen, M., I. Bethke, J. Debernard, T. Iversen, A. Kirkevåg, Ø. Seland, H. Drange, C. Roelandt, I. Seierstad, and C. Hoose (2013), The Norwegian Earth System Model, NorESM1-M-Part 1: Description and basic evaluation of the physical climate, Geoscientific Model Development, 6, 687-720.

Cuo, L., D. P. Lettenmaier, B. V. Mattheussen, P. Storck, and M. Wiley (2008), Hydrologic prediction for urban watersheds with the Distributed Hydrology–Soil–Vegetation Model, Hydrological Processes, 22(21), 4205-4213.

Cuo, L., D. P. Lettenmaier, M. Alberti, and J. E. Richey (2009), Effects of a century of land cover and climate change on the hydrology of the Puget Sound basin, Hydrological Processes, 23(6), 907-933.

Cuo, L., T. K. Beyene, N. Voisin, F. Su, D. P. Lettenmaier, M. Alberti, and J. E. Richey (2011), Effects of mid‐twenty‐first century climate and land cover change on

the hydrology of the Puget Sound basin, Washington, Hydrological Processes, 25(11), 1729-1753.

Dietz, Michael E. (2007), Low impact development practices: A review of current research and recommendations for future directions, Water, Air, & Soil Pollution, 186(1-4), 351-363.

Easterling, D. R., G. A. Meehl, C. Parmesan, S. A. Changnon, T. R. Karl, and L. O. Mearns (2000), Climate extremes: Observations, modeling, and impacts, Science, 289(5487), 2068-2074.

Fry, J. A., G. Xian, S. Jin, J. A. Dewitz, C. G. Homer, Y. LIMIN, C. A. Barnes, N. D. Herold, and J. D. Wickham (2011), Completion of the 2006 national land cover database for the conterminous United States, Photogrammetric Engineering and Remote Sensing, 77(9), 858-864.

Grove, M., J. Harbor, B. Engel, and S. Muthukrishnan (2001), Impacts of urbanization on surface hydrology, Little Eagle Creek, Indiana, and analysis of LTHIA model sensitivity to data resolution, Physical Geography, 22(2), 135-153.

Hawkins, E., and R. Sutton (2011), The potential to narrow uncertainty in projections of regional precipitation change, Climate Dynamics, 37(1-2), 407-418.

Hidalgo, H. G., M. D. Dettinger, and D. R. Cayan (2008), Downscaling with constructed analogues: Daily precipitation and temperature fields over the United States, California Energy Commission PIER Final Project Report CEC-500-2007-123.

Homer, C., J. Dewitz, J. Fry, M. Coan, N. Hossain, C. Larson, N. Herold, A. McKerrow, J. N. VanDriel, and J. Wickham (2007), Completion of the 2001 National Land

Cover Database for the Counterminous United States, Photogrammetric Engineering and Remote Sensing, 73(4), 337-341.

Iversen, T., M. Bentsen, I. Bethke, J. Debernard, A. Kirkevåg, Ø. Seland, H. Drange, J. Kristjansson, I. Medhaug, and M. Sand (2013), The Norwegian Earth System Model, NorESM1-M-Part 2: Climate response and scenario projections, Geoscientific Model Development, 6, 389-415.

Jarvis, A., H. I. Reuter, A. Nelson, and E. Guevara (2008), Hole-filled SRTM for the globe Version 4, available from the CGIAR-CSI SRTM 90m Database: http://srtm.csi.cgiar.org.

Jha, M., Z. Pan, E. S. Takle, and R. Gu (2004), Impacts of climate change on streamflow in the Upper Mississippi River Basin: A regional climate model perspective, Journal of Geophysical Research: Atmospheres (1984–2012), 109(D9).

Jin, S., L. Yang, P. Danielson, C. Homer, J. Fry, and G. Xian (2013), A comprehensive change detection method for updating the national land cover database to circa 2011, Remote Sensing of Environment, 132, 159-175.

Kondoh, A., and J. Nishiyama (2000), Changes in hydrological cycle due to urbanization in the suburb of Tokyo Metropolitan Area, Japan, Advances in Space Research, 26(7), 1173-1176.

Livneh, B., E. A. Rosenberg, C. Lin, B. Nijssen, V. Mishra, K. M. Andreadis, E. P. Maurer, and D. P. Lettenmaier (2013), A Long-Term Hydrologically Based Dataset of Land Surface Fluxes and States for the Conterminous United States: Update and Extensions*, Journal of Climate, 26(23), 9384-9392.

Marengo, J. A., R. Jones, L. M. Alves, and M. C. Valverde (2009), Future change of temperature and precipitation extremes in South America as derived from the PRECIS regional climate modeling system, International Journal of Climatology, 29(15), 2241-2255.

Maurer, E. P., L. Brekke, T. Pruitt, and P. B. Duffy (2007), Fine‐resolution climate projections enhance regional climate change impact studies, Eos, Transactions American Geophysical Union, 88(47), 504-504.

Maurer, E., and H. Hidalgo (2008), Utility of daily vs. monthly large-scale climate data: an intercomparison of two statistical downscaling methods, Hydrology and Earth System Sciences, 12(2), 551-563.

Maurer, E., H. Hidalgo, T. Das, M. Dettinger, and D. Cayan (2010), The utility of daily large-scale climate data in the assessment of climate change impacts on daily streamflow in California, Hydrology and Earth System Sciences, 14(6), 1125-1138.

Miller, D. A., and R. A. White (1998), A conterminous United States multilayer soil characteristics dataset for regional climate and hydrology modeling, Earth Interactions, 2(2), 1-26.

Murphy, J. M., D. M. Sexton, D. N. Barnett, G. S. Jones, M. J. Webb, M. Collins, and D. A. Stainforth (2004), Quantification of modelling uncertainties in a large ensemble of climate change simulations, Nature, 430(7001), 768-772.

New, M., and M. Hulme (2000), Representing uncertainty in climate change scenarios: a Monte-Carlo approach, Integrated Assessment, 1(3), 203-213.

Olivera, F., and B. B. DeFee (2007), Urbanization and Its Effect On Runoff in the Whiteoak Bayou Watershed, Texas1, JAWRA Journal of the American Water Resources Association, 43(1), 170-182.

Price, C. V., N. Nakagaki, K. J. Hitt, and R. M. Clawges (2006), Enhanced historical land-use and land-cover data sets of the US Geological Survey, US Department of the Interior, US Geological Survey.

Rahman, M. A., D. Armson, and A. R. Ennos (2014), Effect of urbanization and climate change in the rooting zone on the growth and physiology of Pyrus calleryana, Urban Forestry & Urban Greening, 13(2), 325-335.

Rappaport, J. (2003), US urban decline and growth, 1950 to 2000, Economic Review-Federal Reserve Bank of Kansas City, 88(3), 15-44.

Reclamation (2013), Downscaled CMIP3 and CMIP5 Climate Projections: Release of Downscaled CMIP5 Climate Projections, Comparison with Preceding Information, and Summary of User Needs. U.S. Department of the Interior, Bureau of Reclamation, Technical Service Center, Denver, Colorado, 116 pp, available at: http://gdo-dcp.ucllnl.org/downscaled_cmip_projections/techmemo/downscaled_climate.pdf.

Schaake, J. C. (1990), From climate to flow, Climate Change and US Water Resources, P. E. Waggoner, Ed., John Wiley, 177-206.

Sheng, J., and J. P. Wilson (2009), Watershed urbanization and changing flood behavior across the Los Angeles metropolitan region, Natural Hazards, 48(1), 41-57.

Stocker, T. F., D. Qin, G.-K. Plattner, M. Tignor, S. K. Allen, J. Boschung, A. Nauels, Y. Xia, V. Bex, and P. M. Midgley (2013), Climate change 2013: The physical science basis, Intergovernmental Panel on Climate Change, Working Group I Contribution to the IPCC Fifth Assessment Report (AR5), Cambridge University Press, 1552 pp.

Texas State Data Center and Office of the State Demographer (2012), Projections of the Population of Texas and Counties in Texas by Age, Sex and Race/Ethnicity for 2010-2050, 28 pp, available at: http://txsdc.utsa.edu/data/TPEPP/Projections/Methodology.pdf.

US Census Bureau (2011), 2010 Census Urban and Rural Classification and Urban Area Criteria. Web. <https://www.census.gov/geo/reference/ua/urban-rural-2010.html>.

Vano, J. A., N. Voisin, L. Cuo, A. F. Hamlet, M. M. Elsner, R. N. Palmer, A. Polebitski, and D. P. Lettenmaier (2010), Climate change impacts on water management in the Puget Sound region, Washington State, USA, Climatic Change, 102(1-2), 261-286.

Vano, J. A., T. Das, and D. P. Lettenmaier (2012), Hydrologic Sensitivities of Colorado River Runoff to Changes in Precipitation and Temperature*, Journal of Hydrometeorology, 13(3), 932-949.

Vogelmann, J. E., S. M. Howard, L. Yang, C. R. Larson, B. K. Wylie, and N. Van Driel (2001), Completion of the 1990s National Land Cover Data Set for the conterminous United States from Landsat Thematic Mapper data and ancillary data sources, Photogrammetric Engineering and Remote Sensing, 67, 650-662.

Weng, Q. (2001), Modeling urban growth effects on surface runoff with the integration of remote sensing and GIS, Environmental Management, 28(6), 737-748.

White, M. D., and K. A. Greer (2006), The effects of watershed urbanization on the stream hydrology and riparian vegetation of Los Penasquitos Creek, California, Landscape and Urban Planning, 74(2), 125-138.

Wigmosta, M. S., L. W. Vail, and D. P. Lettenmaier (1994), A distributed hydrology‐vegetation model for complex terrain, Water Resources Research, 30(6), 1665-1679.

Wood, A. W., E. P. Maurer, A. Kumar, and D. P. Lettenmaier (2002), Long‐range experimental hydrologic forecasting for the eastern United States, Journal of Geophysical Research: Atmospheres (1984–2012), 107(D20), ACL 6-1-ACL 6-15.

Wood, A. W., L. R. Leung, V. Sridhar, and D. Lettenmaier (2004), Hydrologic implications of dynamical and statistical approaches to downscaling climate model outputs, Climatic Change, 62(1-3), 189-216.

APPENDIX A

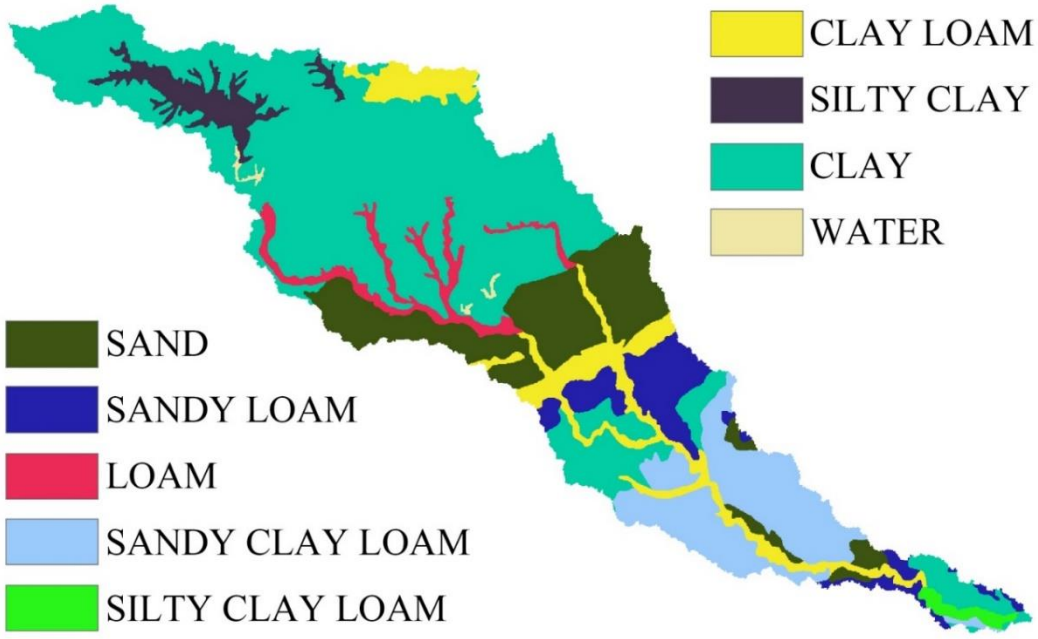

Figure A-1. Soil texture of the San Antonio River Basin.

APPENDIX B

To approximately represent different levels of urbanization process with the San Antonio River Basin, several historical and future land cover maps were created based on the existing datasets, which include land cover types of 1970s, 1992, 2001, 2006, and 2011. In the SARB, the urbanized land surface is mostly contributed to by the City of San Antonio. Thus, in order to study the effect of urbanization, the urban area of San Antonio was recomposed to create land cover maps with an assumption that no land cover type changes occur on non-urban areas.

For historical land cover maps, an existing land cover map from the 1970s was selected as the base map. First, a land cover map without any impervious area was created. This was achieved by removing the urban area from the base map and refilling it with other land cover types based on spatial characteristics and overall percentages of non-urban land cover types. Next, the available historical city maps (1929, 1958, and 1964) were geo-referenced and employed to delineate the profiles of historical urban areas of San Antonio. These profiles were then merged with the non-urban land cover map to obtain the integrated land cover products.

For future land cover maps, the existing land cover map in 2011 (LC2011) was selected as the base map. The future urban areas (in the 2030 and 2080) were estimated based on a population-urban area relationship and projected census data. The population-urban area relationship (Figure 1b) was developed based on the population and city land areas data from 1960 to 2010 provided by United States Census Bureau (USCB) and

Rappaport (2003). Then coefficients were obtained with the fitting method of least squares.

$$UrA = 389.4325 \times \ln(P - 88.2245) - 5025.9364 \qquad \text{(B-1)}$$

where UrA is the urban area (km^2) and P is the population of the City of San Antonio. Total population for the years 2030 and 2080 was estimated using the method used in the Texas Population Projections Program report (Texas State Data Center, 2012). Using equation B-1, the urban areas of 2030 and 2080 were then estimated. Basically, expansion was conducted using the concentric method based around the center of the City (San Antonio). After the completion of this expansion process, the new maps were resampled to 200m resolution and then merged with the non-urban land cover map to keep the consistency of non-urban areas.

Through the methods mentioned above, new land cover maps including non-urban, 1929, 1958, 1964, 2030, and 2080 were produced to support further analysis of urbanization effects on streamflows over the SARB.

APPENDIX C

Generally, soil moisture is highly correlated with soil texture because of various properties such as hydraulic conductivity, porosity, and thermal capacity (and others). For instance, silt loam soil can hold more water than clay soil, while clay can hold more than sandy soil. However, land cover types can also affect soil moisture significantly because of the interactions between the surface vegetation and soil water. Absorption of water from the soil is essential for vegetation to maintain its metabolic activities. But vegetation will not hold this amount of water permanently. Through the process of transpiration, large amounts of water will be released to the atmosphere. The transpiration magnitude is dependent upon vegetation type, temperature, wind speed, etc.

Because the urbanization will remarkably increase impervious areas (and decrease vegetation coverage), the water flux from the soil to the atmosphere is largely inhibited. Thus, if this process outweighs the reduced infiltration rate, the soil moisture will tend to be larger. In order to determine the relationship between different land cover types (mainly with regard to urban areas in this study) and soil moisture, a statistical analysis was conducted using data from the TAMU North American Soil Moisture Database (http://soilmoisture.tamu.edu/). First, soil moisture data from 1290 in-situ stations were acquired from this database. Because these stations belong to different networks, the measurements were conducted at different soil depths and in different periods. Thus, to keep consistency, we calculated the average soil moisture for the top 100 centimeters for the stations that have data spanning (at least) 5 consecutive years. In

addition, only stations with a maximum depth greater or equal to 75 centimeters were selected. Then weighting factors were assigned to each point measurement to obtain the average value (Equation C-1).

$$S = \frac{1}{100}\left\{S_1 \times \left(\frac{d_1+d_2}{2} - 0\right) + S_2 \times \left(\frac{d_2+d_3}{2} - \frac{d_1+d_2}{2}\right) + S_3 \times \left(\frac{d_3+d_4}{2} - \frac{d_2+d_3}{2}\right) + \cdots + S_{n-1} \times \left[\frac{d_{n-1}+d_n}{2} - \frac{d_{n-2}+d_{n-1}}{2}\right] + S_n \times \left[100 - \frac{d_{n-1}+d_n}{2}\right]\right\} \quad \text{(C-1)}$$

where d_i and S_i are the depths and actual values for point soil moisture measurements at station i.

To get the corresponding land cover type associated with the stations, the station locations were overlaid onto the NLCD 2006 land cover map. Then a 500 meter circular buffer area was created for each station. To obtain the dominant land cover type within the circular area, quantities of each land cover type were counted and the maximum value was subsequently chosen. Finally, soil moisture values were averaged based on the stations dominant land cover type. Results are summarized in Table C-1.

Table C-1. Average soil moisture (100 cm) for 249 stations across U.S.

Land cover type	Stations	Average soil moisture (%)
Water	2	19.16%
Developed	17	29.49%
Barren	0	-
Forest	49	24.62%
Shrubland	22	19.61%
Herbaceous	55	24.13%
Planted/Cultivated	96	28.65%
Wetlands	8	25.94%

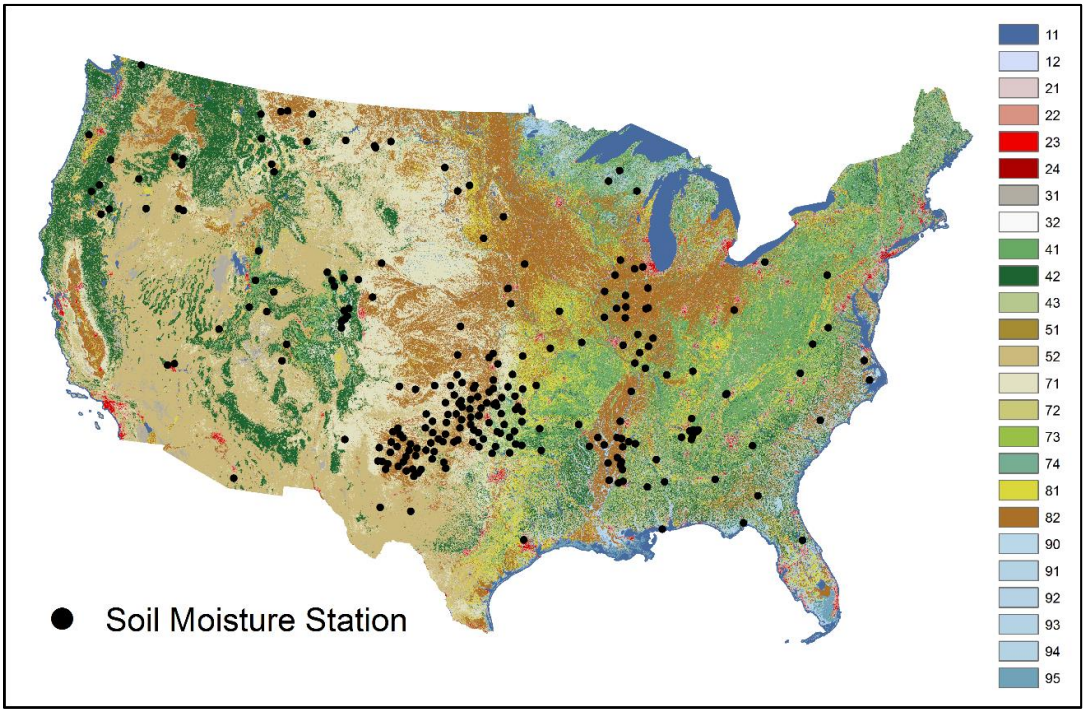

Figure C-1. Selected soil moisture stations in the Continental United States (with maximum depth no less than 75 centimeters and soil moisture data at least 5 consecutive years). Base map is NLCD 2006, with the legend from www.mrlc.gov/nlcd06_leg.php.

There are 249 stations (Figure C-1) chosen for evaluation. As shown in Table C-1, soil moisture values in developed areas (Open Space, Low Intensity, Medium Intensity, and High Intensity) are larger than those for other land cover types—which effectively shows the effect of urbanization on soil moisture. Average soil moisture values for undeveloped areas (Open Space and Low Intensity) and highly developed areas (Medium Intensity and High Intensity) are 29.78% and 24.79%, respectively. This can be attributed to the reduction of infiltration in highly developed areas.